Supplementary Information

Novel self-healing and multi-stimuli-responsive supramolecular gel based on D-sorbitol diacetal for Multifunctional applications

Fuqiang Wen,‡[a] Jingjing Li,‡[b] Lei Wang,[a] Fei Li,[a] Haiyang Yu,[a] Binglong Li[a] Kaiqi Fan,*[c] and Xidong Guan*[a]

Table of contents: **Pages**

1. Experimental section

1.1 Materials

Sorbitol, p-methoxybezaldehyde, p-toluenesulfonic acid monohydrate, the Al nano-powder and the base oils including liquid paraffin, polyethylenglycol (PEG400) and triethylene glycol were purchased from Shanghai Aladdin Bio-Chem Technology Co., Ltd. Alkylated naphthalenes (ANs) were purchased from NacoSynthetics Co., Ltd. 150BS and polyalphaolefin(PAO10) were purchased from ExxonMobil chemical reagent Co., Ltd. Multiple-alkylated cyclopentane (MACS) were purchased Karamay Petrochemical Co., Ltd. High-energy density hydrocarbon fuel JP-10 was purchased from Heowns Biochem Technologies LL. Tianjin. The chemical reagents were commercially available and directly utilized without further purification.

1.2 Instrumentation

NMR experiments: All NMR studies were performed on a Bruker DPX 400 MHz spectrometer.

Mass spectrometry: Mass spectra were recorded on a mior OTOF-QII high-resolution mass spectrometer.

Field Emission Scanning Electron Microscope (FESEM): The morphologies of the xerogels were obtained by a Hitachi S-4800 SEM instrument operating at 3-5kV. Samples were prepared by dropping the diluted solution of gels on the thin aluminum sheets and then dried under vacuum for 24 h. We coated the samples with a thin layer of Au before the experiment.

FT-IR spectroscopy: IR spectra were collected by a FTS3000 spectrometer with KBr pellets.

UV spectroscopy: UV spectroscopy was performed on a UV-1800PC spectrophotometer. The path length of the quartz cell was 10 mm.

Powder X-ray diffraction (PXRD): Powder X-ray diffraction (XRD) diagrams of xerogels were obtained using Bruker D8-S4 (Cu Kα radiation, $\lambda = 1.546$ Å). The d spacing values were calculated by Bragg's law ($n\lambda = 2d \sin\theta$).

Rheology measurements: Rheology experiments were carried out with a strain

controlled rheometer (Anton Paar Physica MCR 301) equipped with steel-coated parallel-plate geometry (15 mm diameter). Dynamic frequency sweep was conducted at 0.1% strain. Dynamic strain sweep was conducted at a constant frequency (1 Hz). Step strain measurement started at a constant strain of 0.1%; then, a following strain of 100% was applied to destroy the sample, and then a constant strain (0.1%) was applied again.

Tribology Test: The tribological tests of gel lubricant and base oil were performed using an Optimol SRV-IV friction and wear tester (applied load: 200N; frequency: 25 Hz; stroke: 1 mm; duration: 30 min; temperature: 25 °C). The corresponding friction coefficient (COF) were recorded with a computer connected to the tester. A MicroXAM-800 3D noncontact surface mapping profiler was used to measure the wear volume of the lower disk.

Gelation test: These tests were performed by adding the weighed amount of G8 into the measured volume of solvent in the tube (10 mm diameter) and then heating the tube until the gelators were dissolved or could not be dissolved ever. A "stable to inversion test tube method" was adopted. Each experiment was done in duplicate.

Gel–sol phase transition temperature measurements (T_{gel}): The gel-sol transition temperature was determined by a conventional ball-drop method. A small glass ball with a diameter of 5 mm (0.24 g) was placed on the top of the gel in a test tube (10 mm diameter) which was in a thermo-stated oil bath and was heated at ca. 1.5 °C /min. The temperature corresponding to be submerged in the solution was regarded as the T_{gel} of the gel. The measured experiments were carried out in duplicate.

DSC experiment: DSC scans were carried out using a TA DSC Q2000 model with a TA Refrigerated Cooling System 90 and heating rate of 5 °C per minute.

TGA analysis: TGA scan was performed on a TGA Q500 V20.13 Build 39, with a maximum temperature of 600 °C and heating rate of 10 °C per minute.

1.3 Chemical Identification of gelator D1.

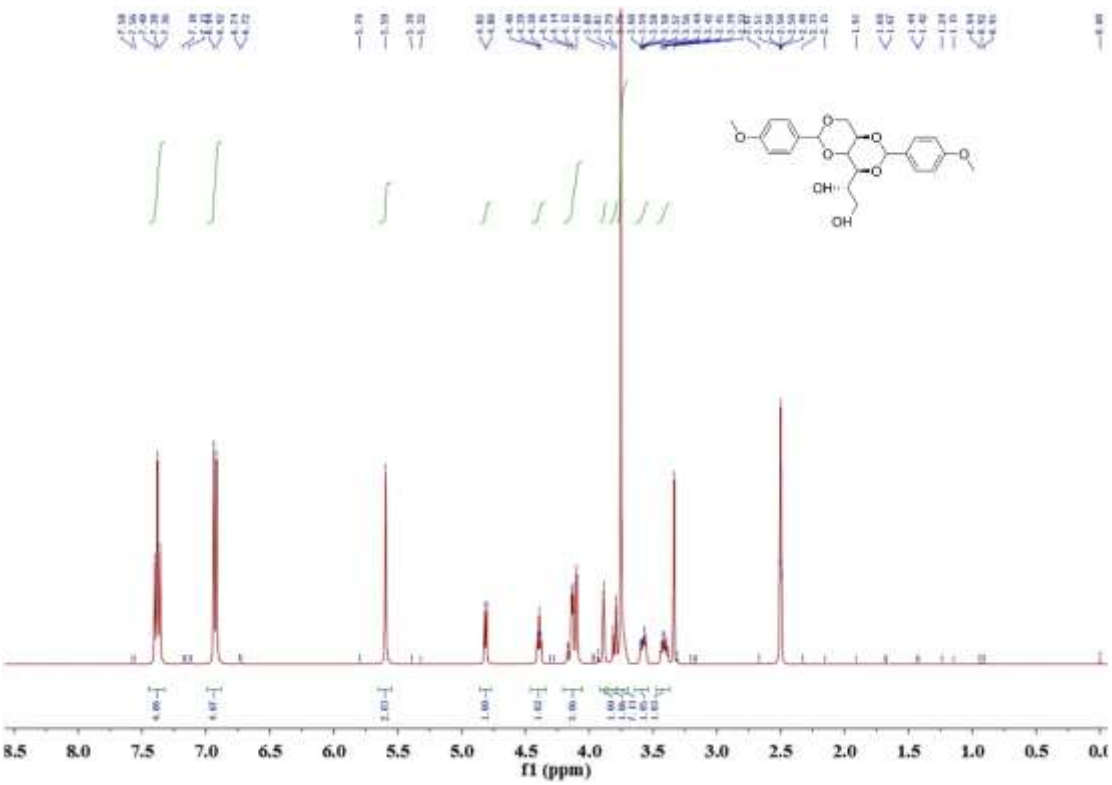

Figure S1. ^{1}H NMR (400 MHz) Spectra of gelator D1 in DMSO-d_6.

^{1}H NMR (400 MHz, DMSO-d_6, δ): δ 7.38 (t, J = 8.3 Hz, 4H; Ar H), 6.93 (d, J = 8.5 Hz, 4H; Ar H), 5.59 (s, 2H; OCHO), 4.81 (d, J = 5.7 Hz, 1H; CHO H), 4.39 (t, J = 5.5 Hz, 1H; CH_2O H), 4.13 (d, J = 5.4 Hz, 2H; CH_2), 4.10 (s, 1H; CH), 3.89 (s, 1H; CH), 3.80 (d, J = 9.3 Hz, 1H； CH), 3.75 (s, 6H; OCH_3), 3.63-3.54 (m, 1H; CH), 3.41 (m, 1H; CH).

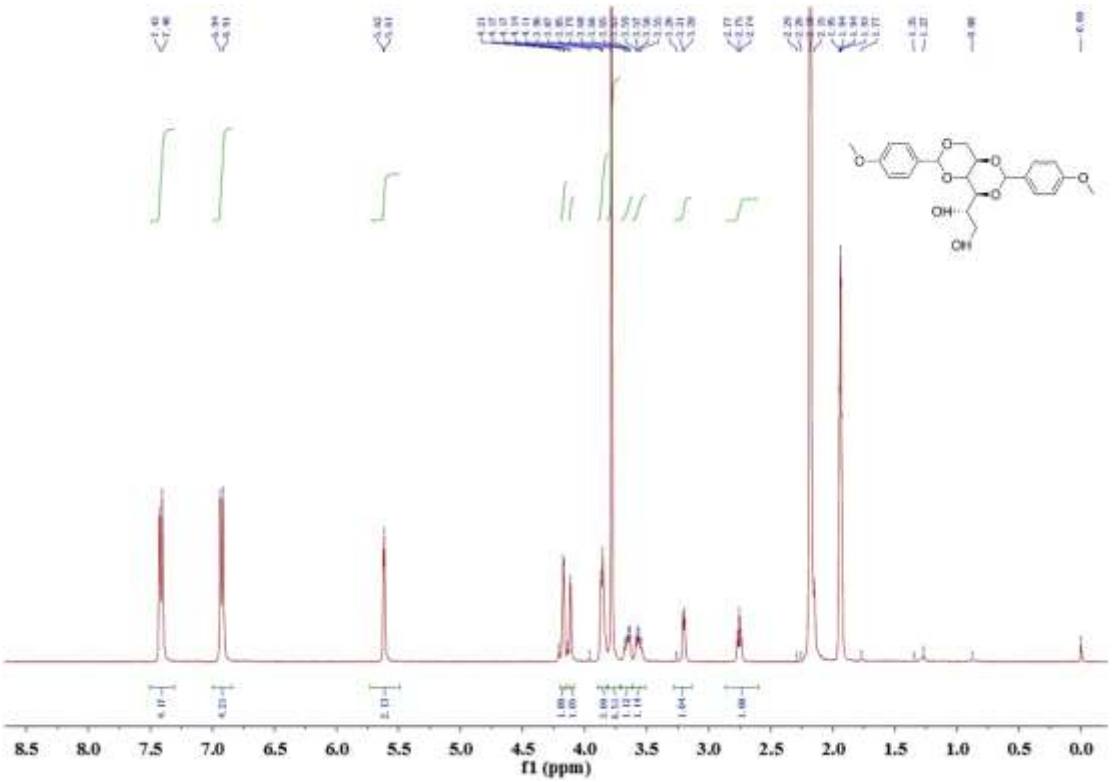

Figure S2. ^{1}H NMR (400 MHz) Spectra of gelator D1 in CD_3CN-d_3.

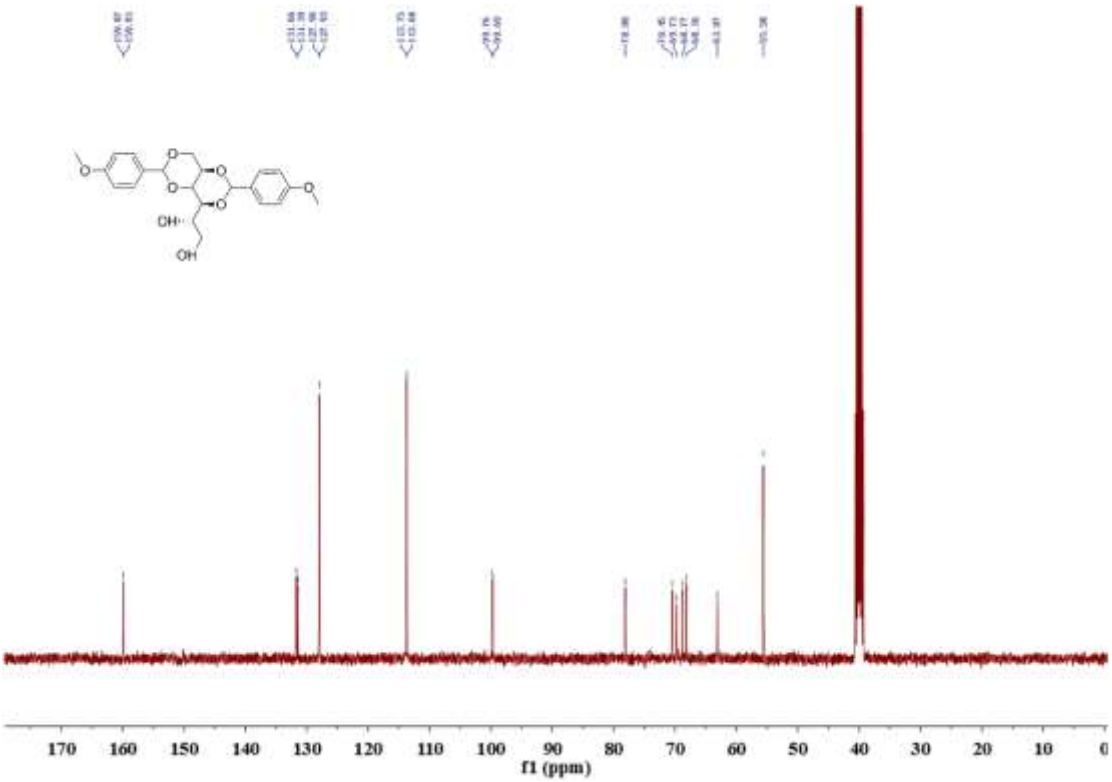

Figure S3. ^{13}C NMR (400 MHz) Spectra of D1 in DMSO-d_6.

^{13}C NMR (101 MHz, DMSO) δ 159.87, 159.81, 131.66, 131.39, 127.96, 127.93, 113.75, 113.68, 99.76, 99.69, 78.08, 70.45, 69.73, 68.77, 68.16, 63.07, 55.58.

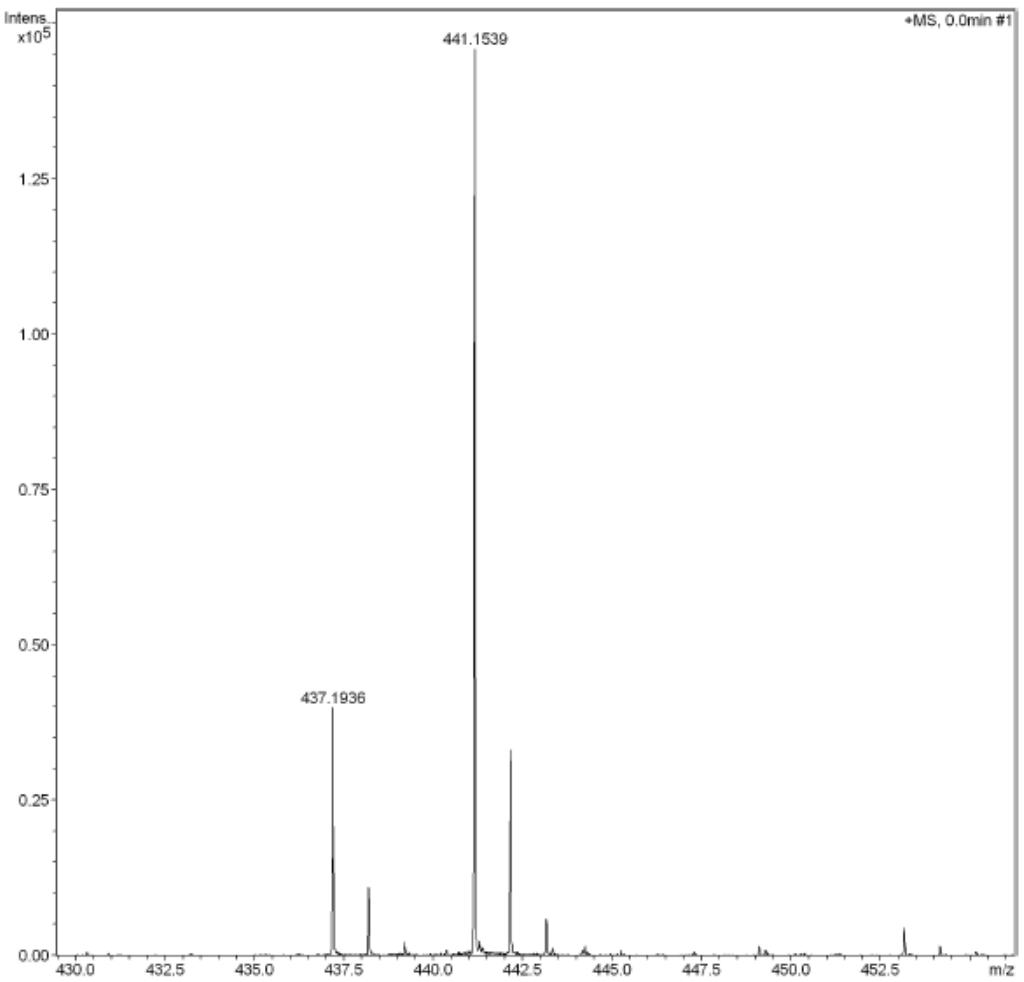

Figure S4. HRMS Spectra of gelator D1.

HRMS (ESI) *m*/*z*: $[M+H]^+$ calcd for $C_{21}H_{23}O_8$, 441.1628; found, 441.1539.

2. Gelation ability of gelator D1

Table S1: Gelation ability results of gelator D1 in various solvents.

Liquids	T_{gel}(℃)	CGC (wt%)	Liquids	T_{gel}(℃)	CGC(wt%)
Acetone	47	TG(0.12)	n-Butyl acetate	105	TG(0.29)
tetrahydrofuran	62	TG(0.53)	o-Xylene	112	TG(0.09)
Acetonitrile	75	OG(0.20)	o-Dichlorobenzene	153	TG(0.08)
Methanol	58	OG(0.80)	Liquid Paraffin	162	OG(0.78)
Ethanol	63	OG(0.31)	ANs	201	OG(0.57)
n-Propanol	82	OG(0.33)	150BS	112	OG(0.83)
Isopropanol	79	OG(0.40)	PAO10	122	OG(0.94)
n-Butanol	97	OG(0.31)	MACS	99	TG(0.68)
n-Octanol	159	OG(0.22)	Triethylene glycol	182	TG(0.88)
Iso-octanol	147	OG(0.19)	JP-10	166	OG(0.81)

OG: opaque gel, TG: transparent gel, ANs: alkylated naphthalenes,
MACS: multiple-alkylated cyclopentane, JP-10: $C_{10}H_{16}$, exo-tetrahydrodicyclopenta-diene.

3. Self-assembly mechanism of gelator D1

3.1 IR spectroscopy

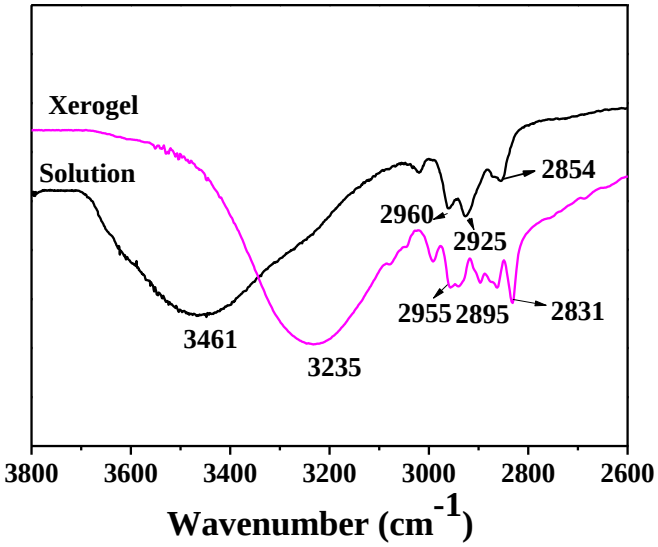

Figure S5. FTIR spectra of chloroform solution (0.1 mM) of D1 and acetonitrile xerogel (1.0% w/v) of D1.

3.2 Concentration and temperature-dependent ^{1}H NMR spectroscopy

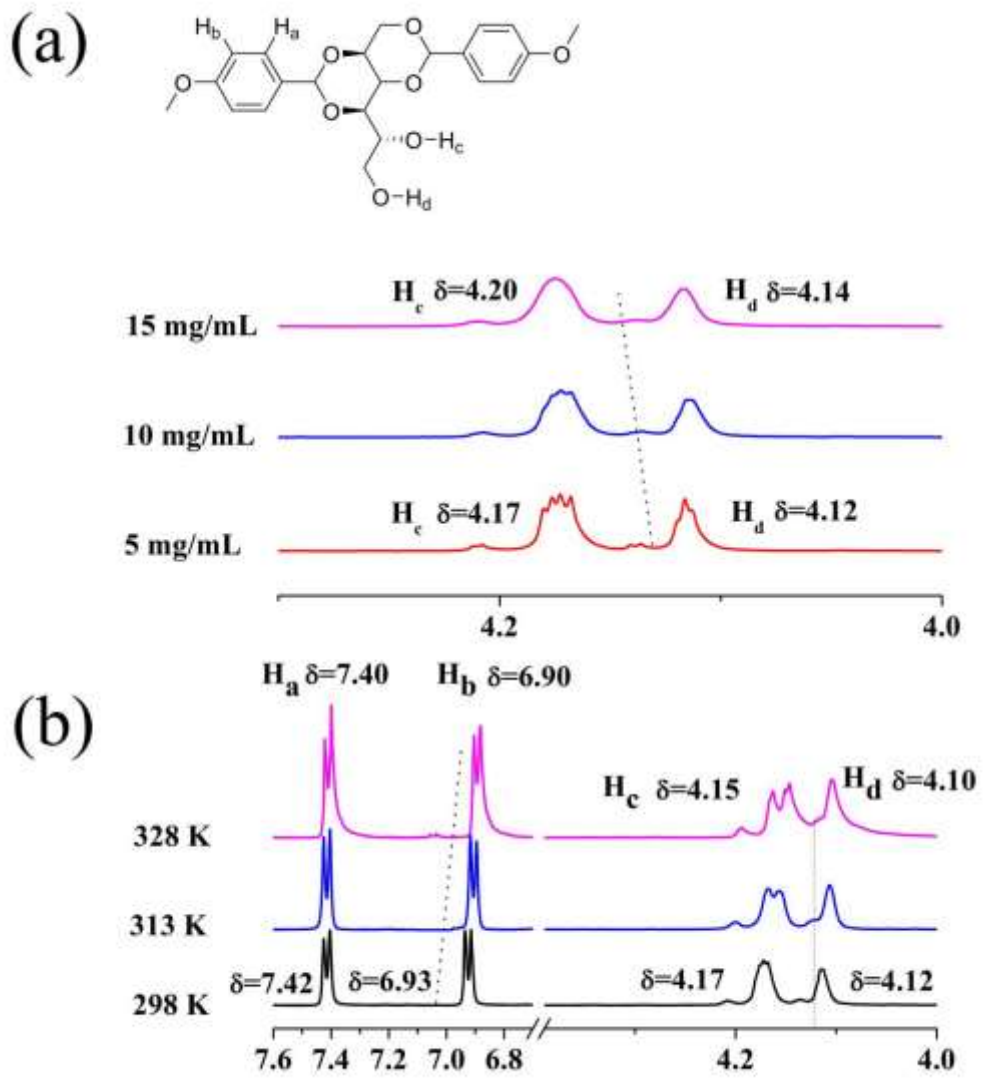

Figure S6. (a) Change in ^{1}H NMR chemical shift of hydroxyl protons of gelator in acetonitrile as concentrations increases from 5 mg/mL to 15 mg/mL at 25 °C. (b) Change in ^{1}H NMR chemical shift of hydroxyl and aromatic protons of gelator in acetonitrile (10 mg/mL) as temperature increases from 25 ℃ to 55 °C.

3.3 X-ray diffraction pattern

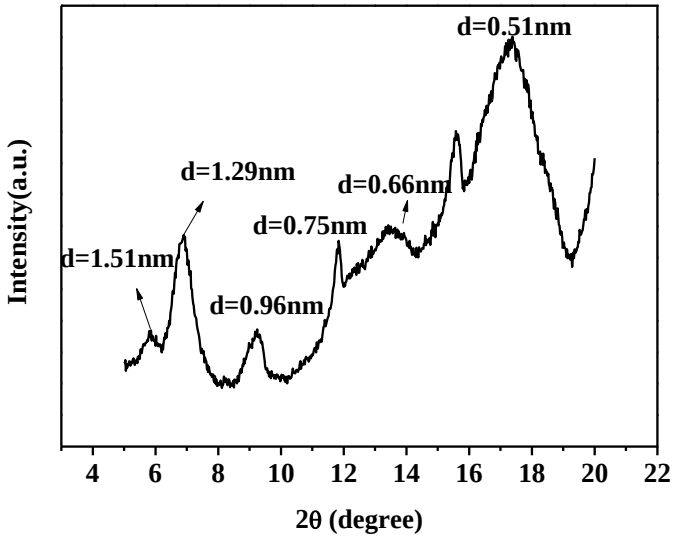

Figure S7. WXRD spectra of D1 xerogel made from acetonitrile (2.0% w/v).

3.4 SEM and TEM images

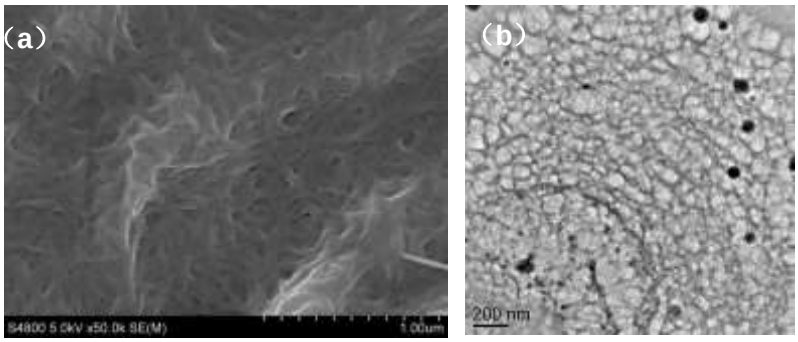

Figure S8. SEM (a) and TEM (b) images of xerogel made from acetonitrile (1.0% w/v).

4. Multi Molecular Recognition

4.1 Chiral recognition mechanism of gels of D1/(acetonitrile: acetone=8:2, 1%, w/v) gels

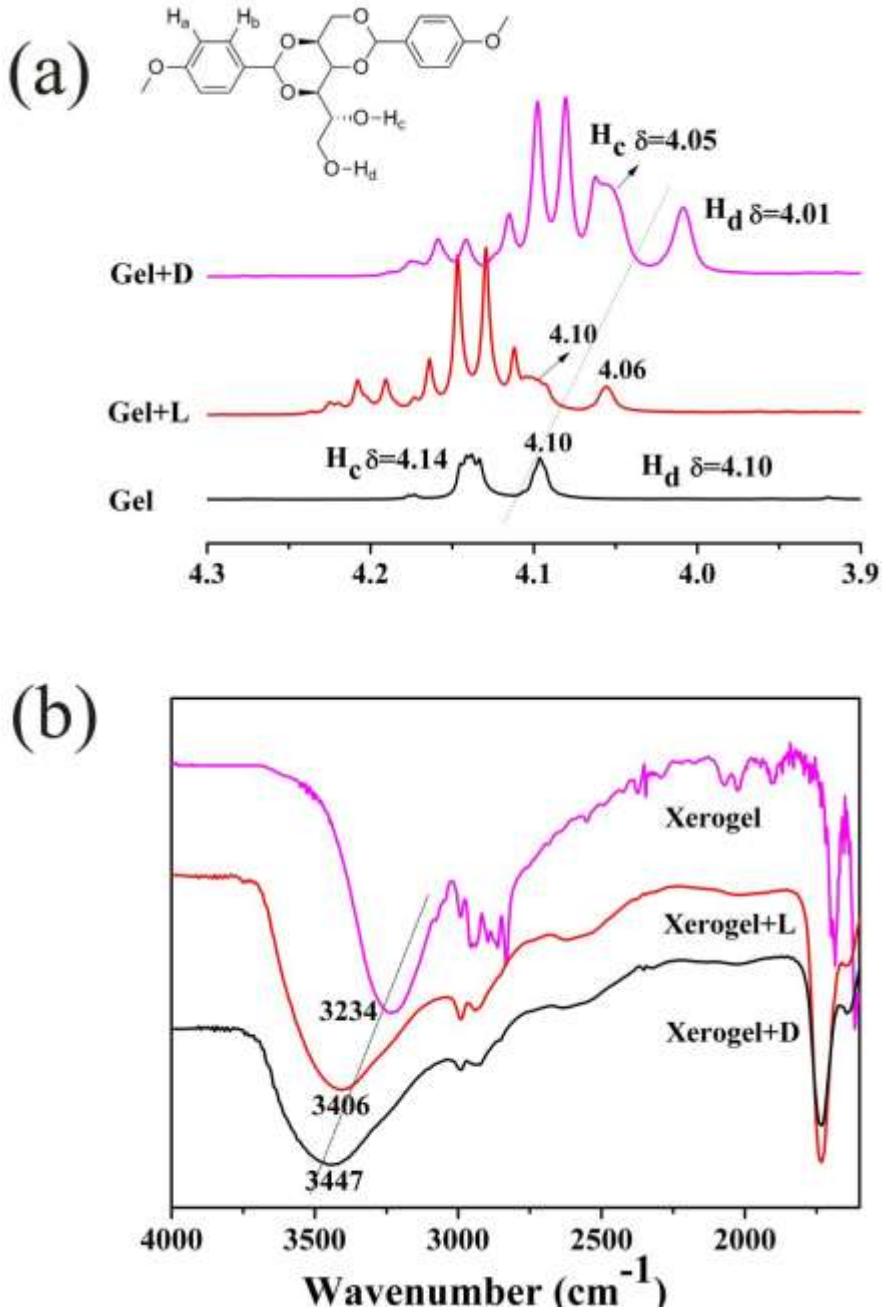

Figure S9. (a) ^{1}H NMR spectra of D1/gels (acetonitrile-d_3: acetone=8:2,1.0% w/v) with D and L-Lactic acid. (b) IR spectra of 1/xerogels(acetonitrile:acetone=8:2,1.0% w/v) with D and L-Lactic acid.

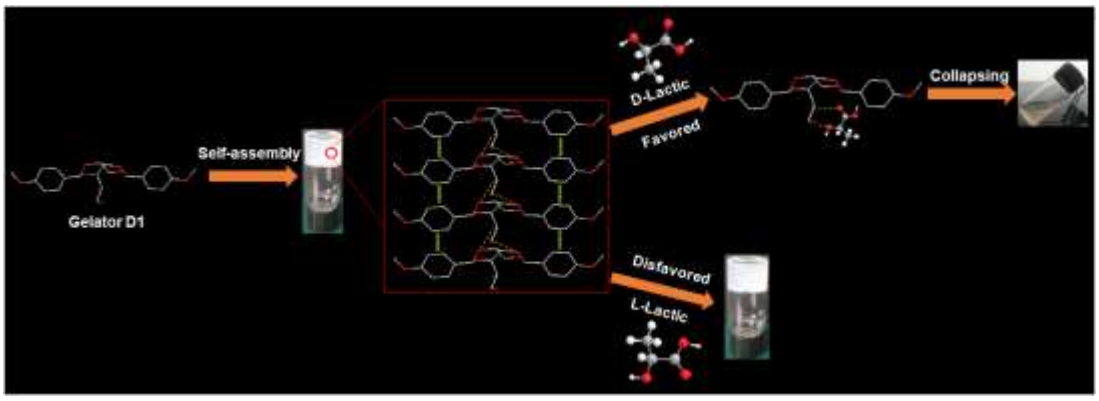

Scheme S1. Proposed mechanism of the molecular recognition of organogel based on gelator D1

4.2 Multi stimuli-responsive mechanism of D1/acetonitrile gel

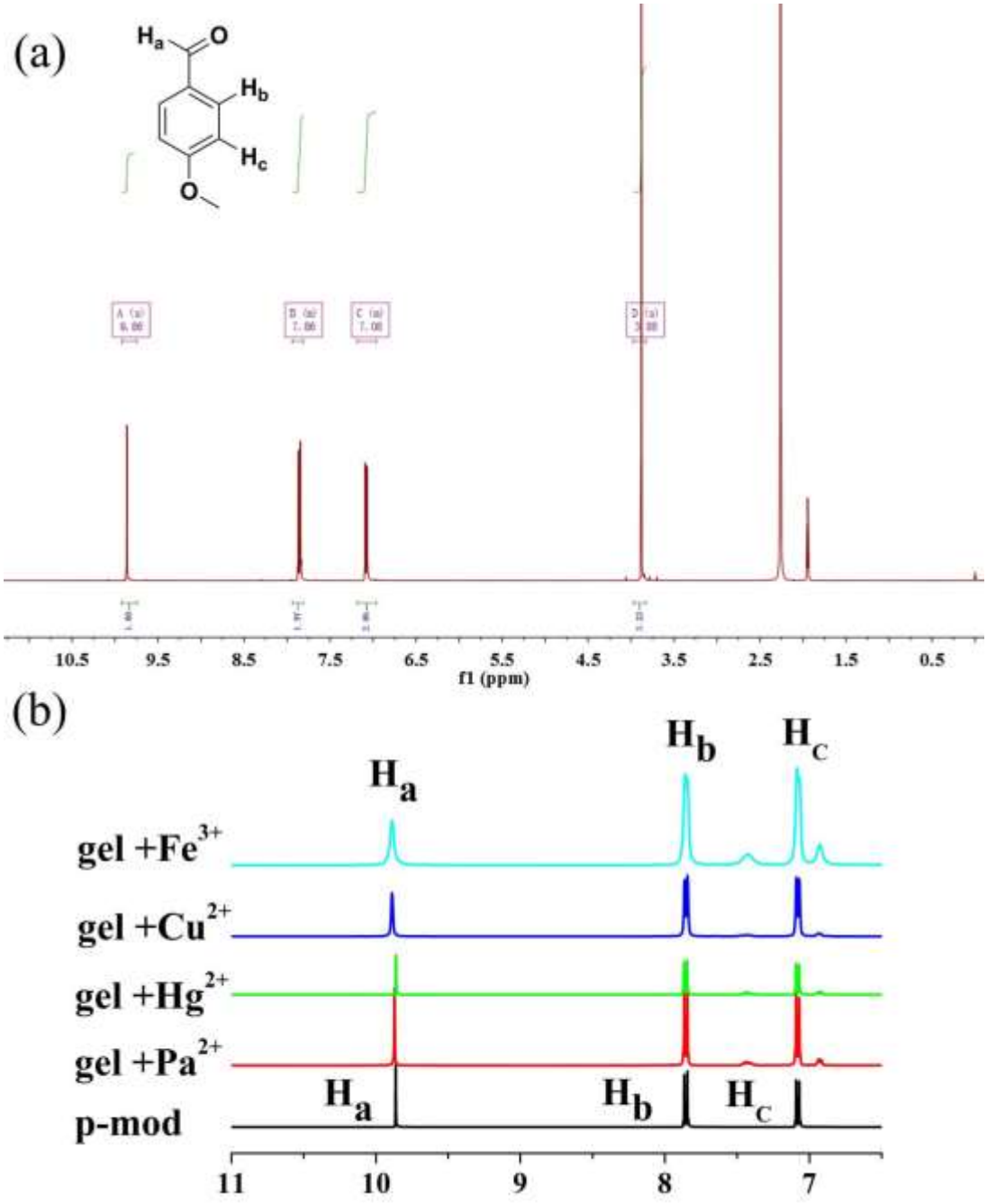

Figure S10. (a) ^{1}H NMR spectra of p-methoxybezaldehyde (p-mod) in acetonitrile-d_3. (b) ^{1}H NMR spectra of D1/acetonitrile-d_3 gels (1.0% w/v) with anions, acid and oxidant.

Possible multi stimuli-responsive mechanism

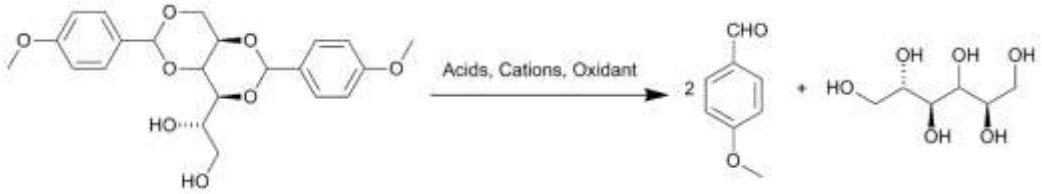

Scheme S2. Illustration of the multi stimuli-responsive mechanism for the D1/ acetonitrile gels.

As shown in Fig. S6 and S10 (ESI†), when a cation, acid, or oxidant agent is added to acetonitrile gel, the signal of p-methoxybezaldehyde appeared (9.89 ppm) and the signal of aromatic protons(7.42 and 6.93 ppm) of gelator D1 disappeared indicating the decomposition of the acetal in gelator.

4.3 The mechanism of discriminate aliphatic and aromatic amines

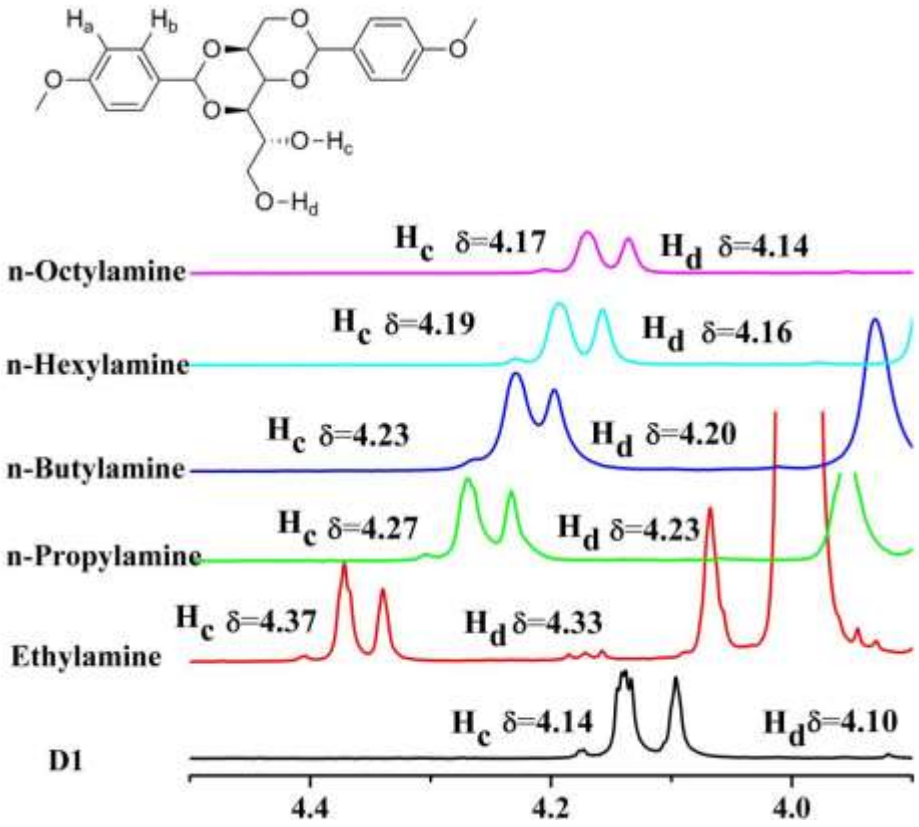

Figure S11. ^{1}H NMR spectra of D1/ gels (acetonitrile-d_3: acetone=8:2,1.0% w/v) with aliphatic amines.

5. Rheology

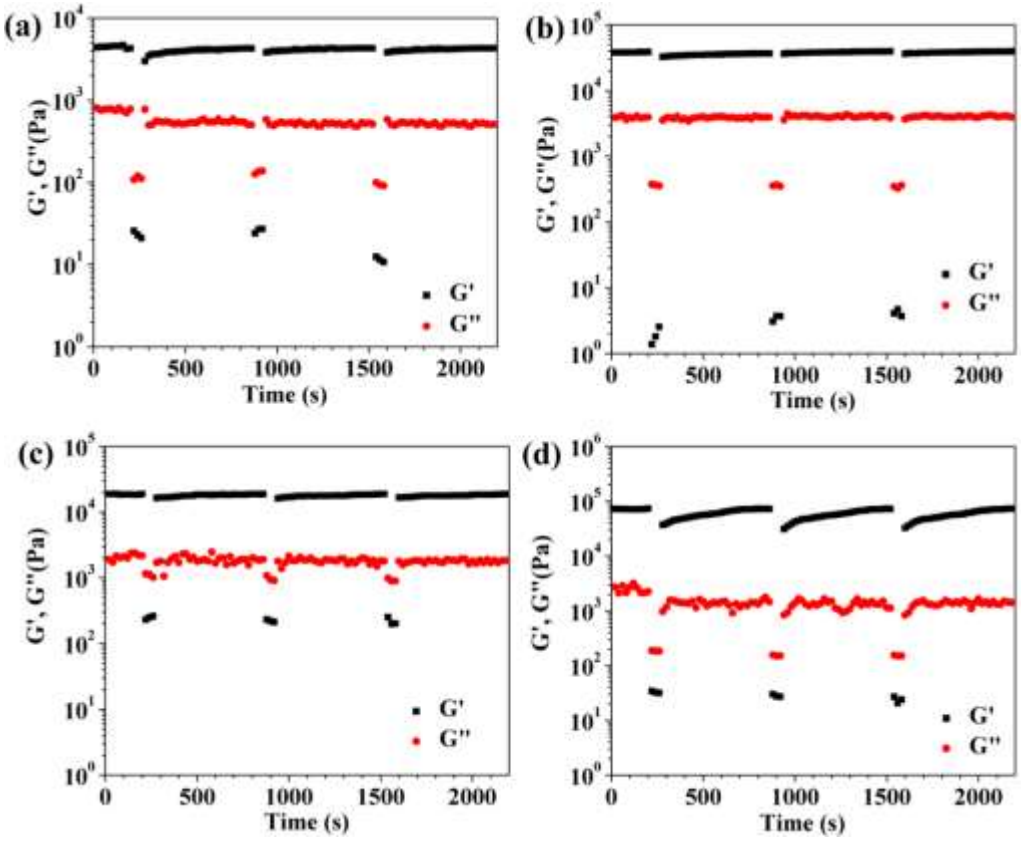

Figure S12. The step strain experimental data obtained from the gels of D1 in various organic solvents (a) Ethanol gel (1.0% w/v), (b) o-Dichlorobenzene gel (1.0% w/v), (c) ANs gel (2.0% w/v) and (d) JP-10 gel (1.0% w/v).

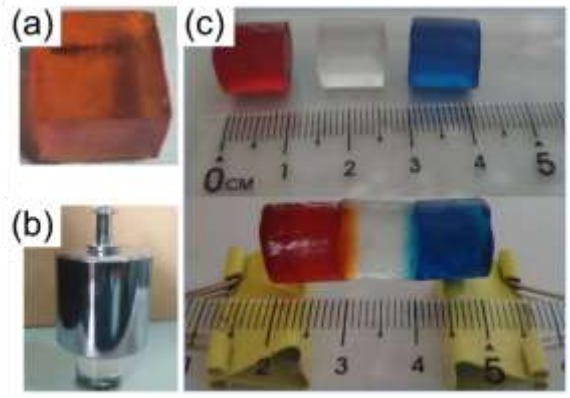

Figure S13. (a) Moldable property of 1 wt% o-dichlorobenzene gel (doped with methyl red). (b) Load-bearing capacity of 1 wt % o-dichlorobenzen gel (the weight is 200 g). (c) Self-healing process of D1/o-dichlorobenzene gel of (1%, w/v).

6 Gel Lubricants

6.1 Thermal Analysis

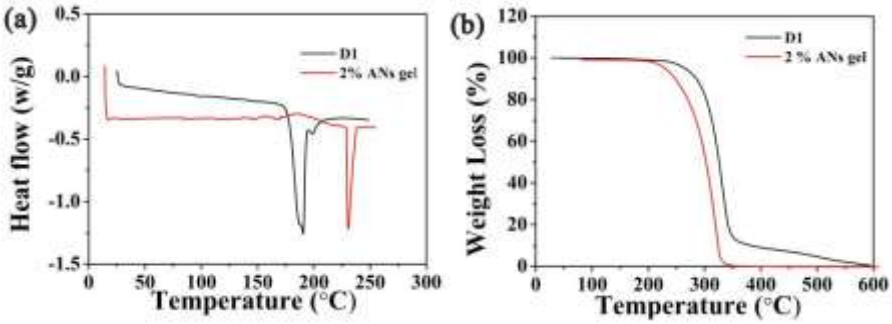

Figure S14. (a) DSC thermograms and (b) TGA graphs of gelator D1 and 2% ANs gel.

6.2 Rheological Characterization

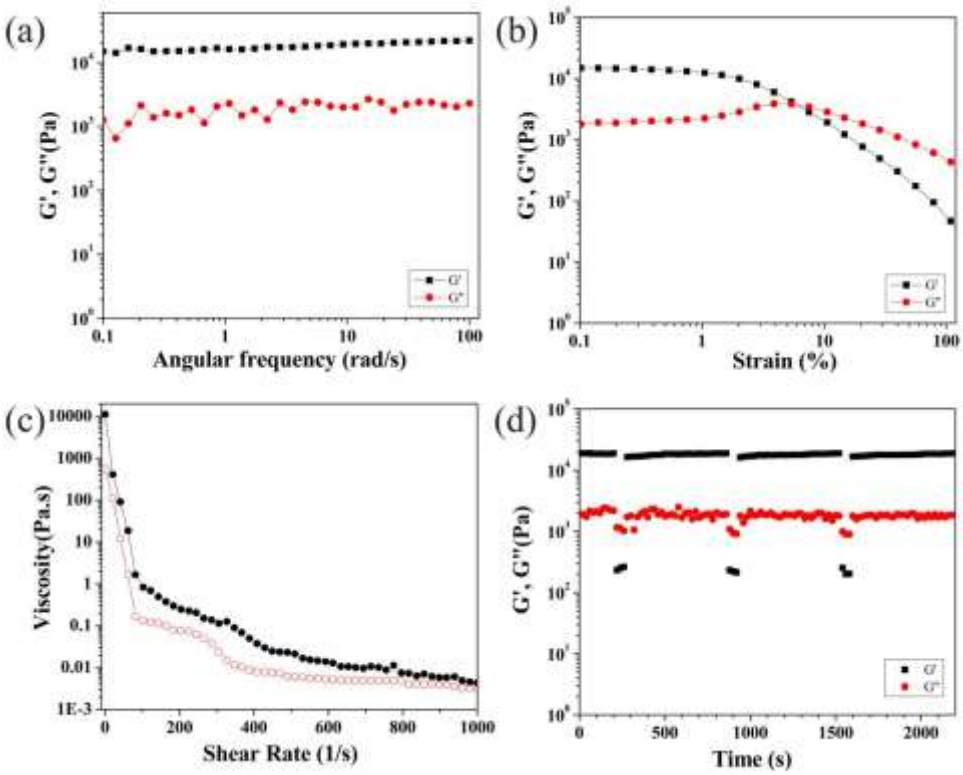

Figure S15.The step strain experimental data obtained from the D1/ANs gels (a)Frequency sweep, with a fixed strain 0.1%. (b) Strain sweep was performed from 0.01% to 100%. (c)Viscosity curves, at shear rates ranging from 0-1000 s^{-1}. at 25 ºC with a 1 Hz. (d) Time scan tests were performed with an alternating strain of 0.1% and 100% with 1 Hz at 25 ºC.

6.3 Lubrication Mechanism.

6.3.1 Corrosion Tests of AISI 52100 Steel

As shown in Figure S16, compared with pure ANs，the steel surface was eroded less severe in ANs gels . EDS elemental analysis (Figure S10, 11) suggest that the ANs gels has less percentage composition of C, N and Cr on the corroded surface of steel immersed in gels than that of ANs base oil, while the percentage composition of Fe are obviously more. The above result illustrates that the ANs gel could slow down the deterioration of base oil and prevent the corrosion of steel efficiently.

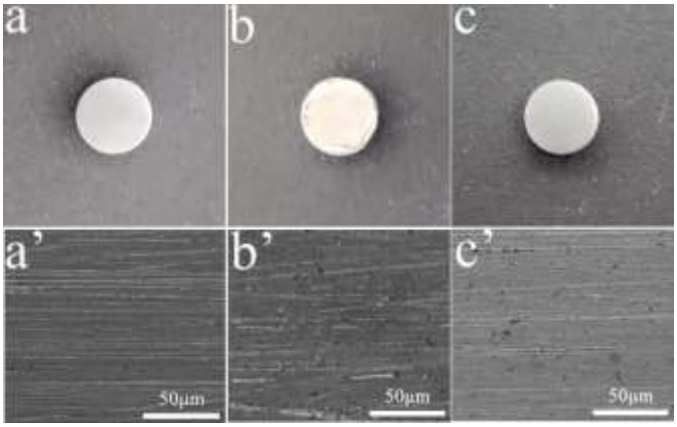

Figure S16. Digital pictures and SEM images of the corrosion surface of AISI 52100 steel immersed in different ANs and 2 wt % ANs gel for 60 days. (a, a') blank, (b, b') immersed in ANs, (c, c') immersed in ANs gel.

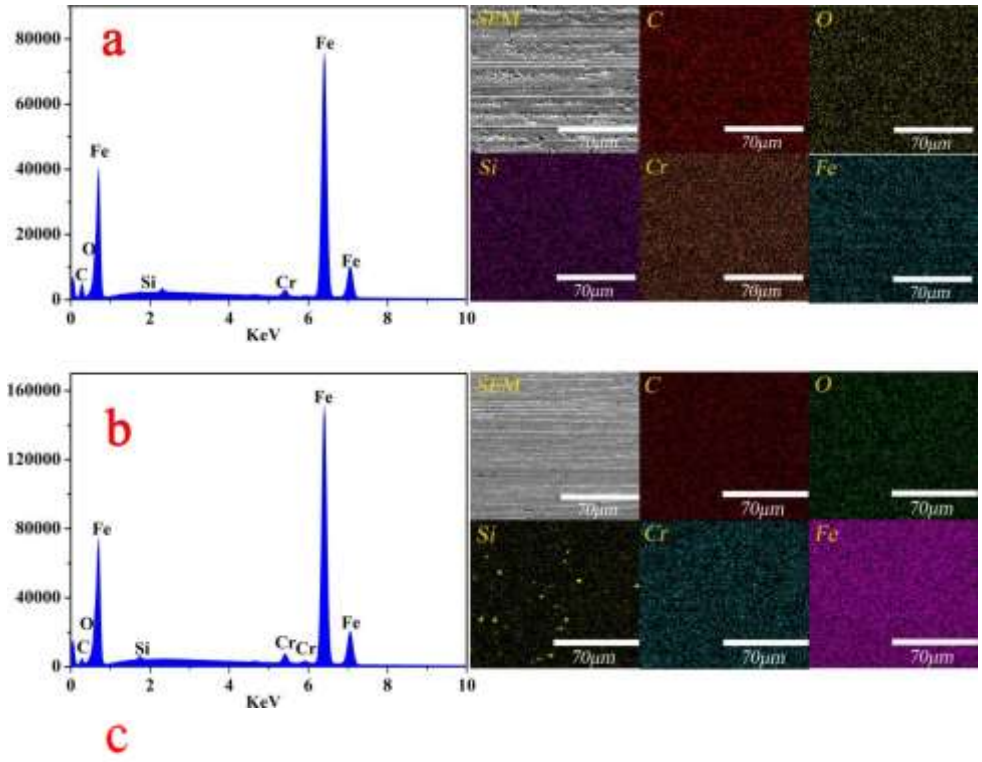

Element	C	O	Si	Cr	Fe
Content(%) (atomic percent) Steel immersed in ANs	37.93	7.86	0.12	0.85	53.24
Content(%) (atomic percent) Steel immersed in ANs gel	22.10	5.52	0.66	1.55	70.17

Figure S17. EDS elemental surface distribution images of the AISI 52100 steel immersed in (a) ANs and (b) 2 wt %ANs gel at 50℃ and air atmosphere (humidity 60%) for 60 days. (c) Content % of the corresponding element.

6.3.2 SEM and 3D Optical Microscopy Images of Wear Scars

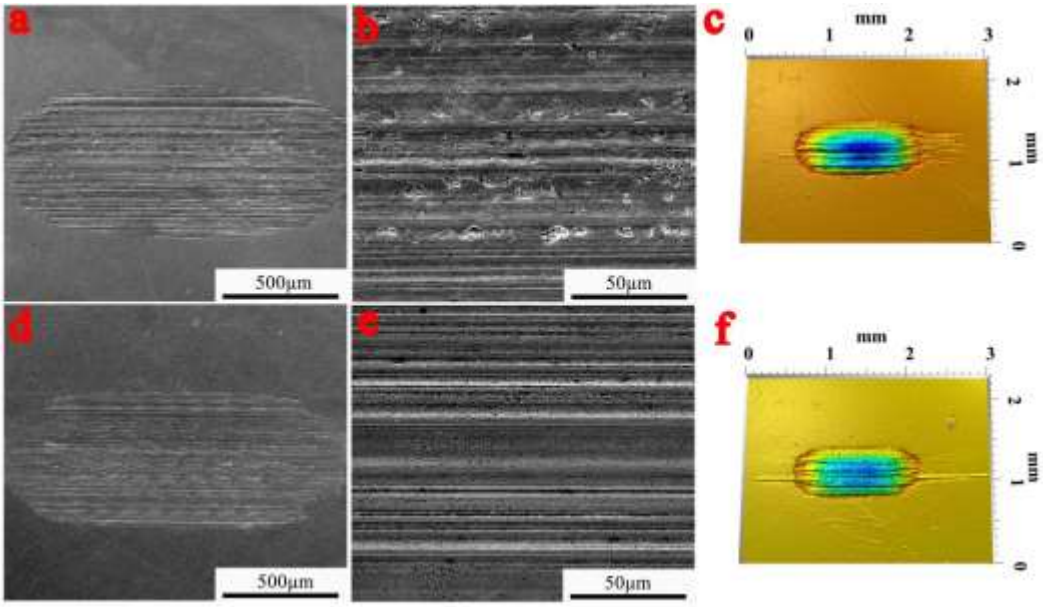

Figure S18. SEM images and corresponding 3D optical microscopy images of the worn surfaces of steel disks lubricated by ANs (a,b and c) and 2 wt % ANs gel at 150℃ (d, e and f).

SEM images and 3D optical microscopy images (Figure S12) reveal that the wear scar lubricated by ANS exhibits severe adhesion and scratches, whereas that lubricated by ANs gel are slight and relatively smooth. This phenomenon may be attributed to the anticorrosion properties of ANs gel preventing corrosive wear.

6.3.3 X-ray Photoelectron Spectroscopy (XPS) Spectra and Contact Resistance Test

It can be seen that the main elements of the worn areas lubricated by ANs and 2 wt % ANs gel were Fe F, O and C. For the surfaces lubricated by ANs and 2 wt % ANs gel l, the peaks of Fe2p appear at 724.10, 709.11 and 725.01, 710.63 eV respectively, the peaks of F1s appear at706.66and 706.48 eV respectively, the peaks of O1s appear at 531.58, 529.38 and 531.74, 529.46 eV respectively, implying the possible existence of Fe2O3, FeOOH, FeF2, and Fe3O4. The peaks of C1s appear at 288.54 and 284.58 eV may be attributed to C-C, C-H bonds in the alkyl groups. The results indicate that a tribofilm formed on the surfaces by the tribochemical reaction. (ECR) measurements were carried out to determine whether an insulating tribofilm was generated. It is observed that the value of ECR lubricated ANs is very low, implying that almost direct contact between rough sliding pairs result in friction and wear. However, a relatively large value of ECR was measured when lubricated by 2% ANs gels. This implies that a comparatively stable insulating tribofilm forms on sliding pairs.

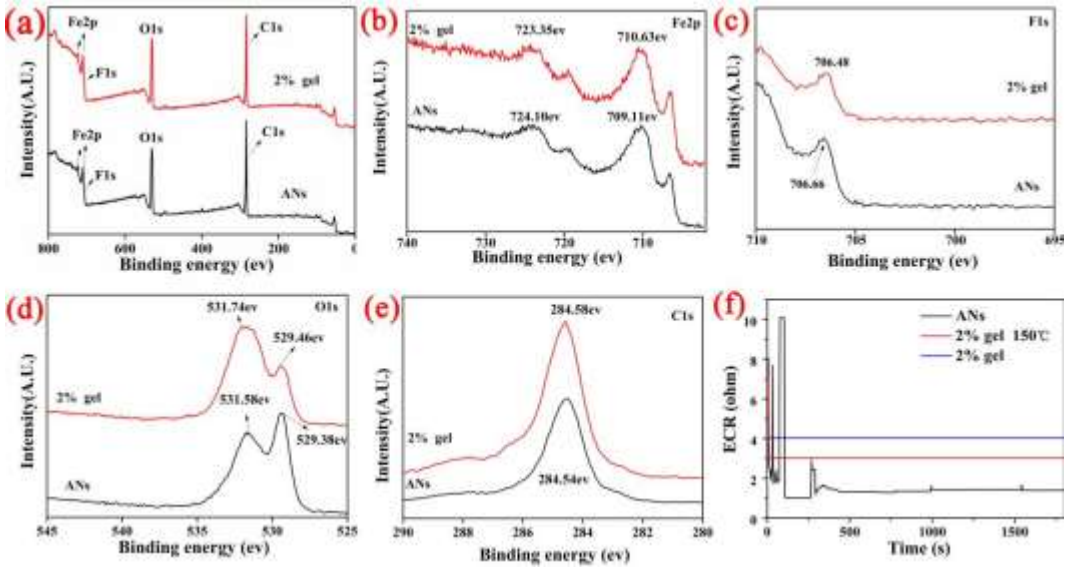

Figure S19. XPS spectra of full scan (a) and high resolution of Fe2p (b), F1s (c), O1s (d) and C1s (e) of the worn surfaces lubricated by ANs and 2 wt% ANs gel at 150℃; (f) contact resistance of steel/steel contacts during friction test.

.

7. Properties of gel fuels

7.1 Efficiency of D1/methanol gel, DSC and TGA graphs

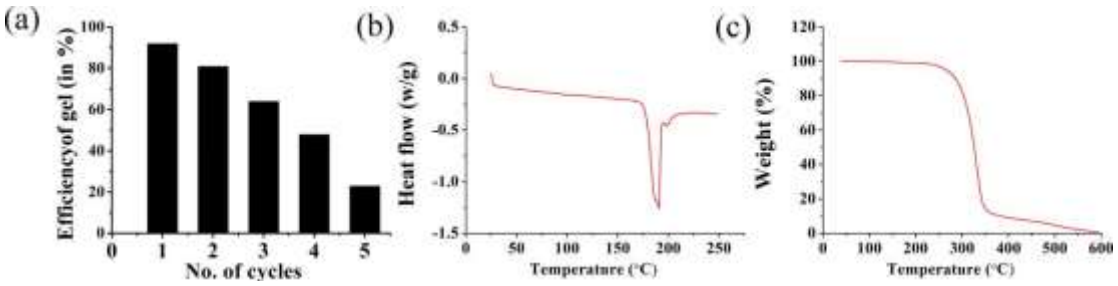

Figure S20. (a) Efficiency of D1/methanol gel after various cycles. (b) DSC thermograms and (c) TGA graphs of gelator D1.

7.2 Efficiency of D1/methanol gel, DSC and TGA graphs

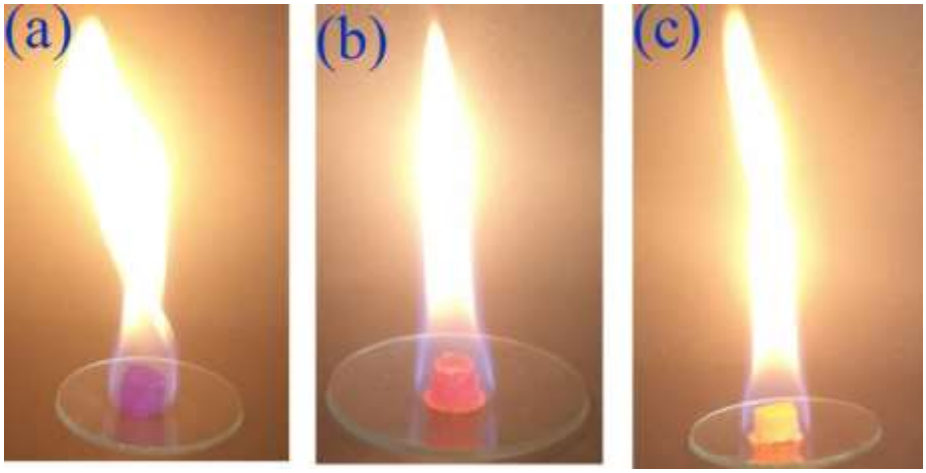

Figure S21. The D1/methanol gels have colored with (a) methyl violet, (b) methyl orange and (c) rhodamine 6G, respectively.

8. Strain sweep tests

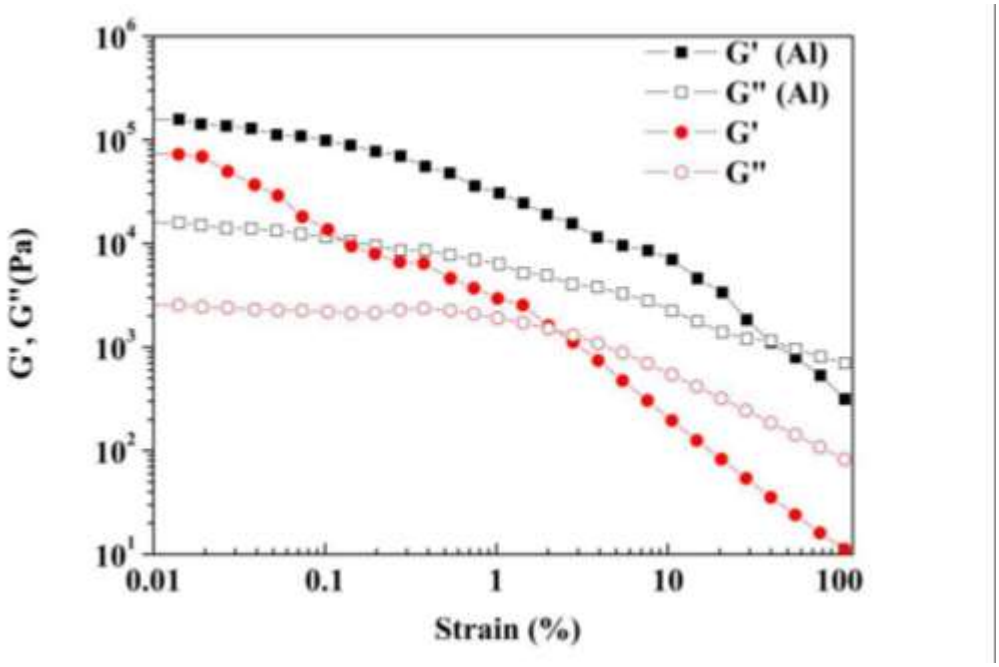

Figure S22. Strain sweep curves of 2 wt% D1 JP-10 gel with or without Al powers (5 wt% Al, 50 nm).

9. Phase-selective gelation of D1 powder

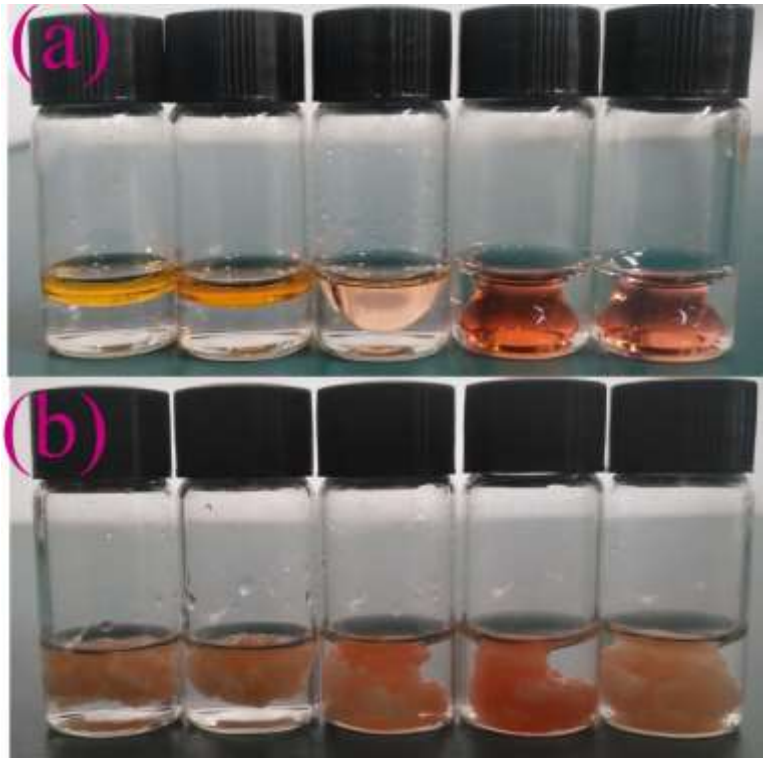

Figure S23. Phase-selective gelation of D1 powder in aldehyde-water mixture at room tempreture (a) Mixture of 1 mL of aldehydes and 3 mL water (from left to right: n-butylaldehyde, octanal, benzaldehyde, salicylaldehyde and p-methoxybezaldehyde). (b) The ability of gelator D1 for phase selective gelation in mixture of 1 mL of aldehydes and 3 mL water (from left to right: n-butylaldehyde, octanal, benzaldehyde, salicylaldehyde and p-methoxybezaldehyde).

Different kinds of aldehyde compounds including n-butylaldehyde, octanal, benzaldehyde, salicylaldehyde and p-methoxybezaldehyde were mixed with water (1 mL/3 mL) respectively, and D1 powders (4.0 wt%) were added. All the tested aldehyde liquids were gelled after 30 min.

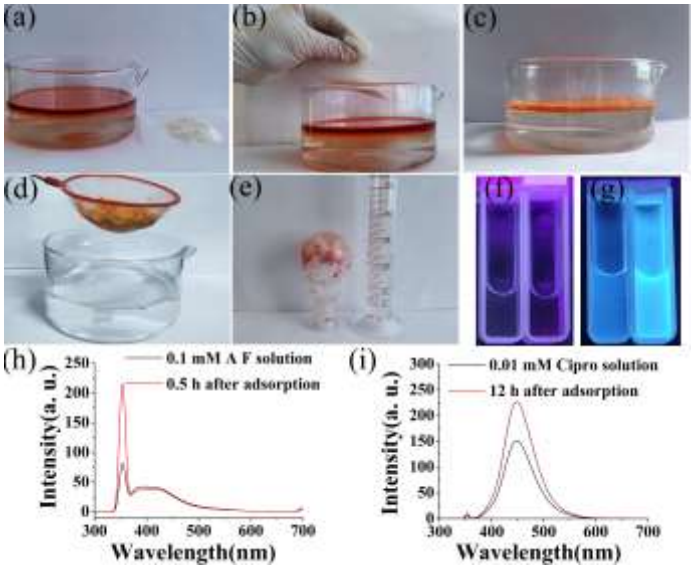

Figure S24 (a) Biphasic mixture of 30 mL octanal (dyed with methyl red) and 300 mL water. (b) Spreading of D1 powders over the layer of octanal. (c) Gelation of the octanal layer after 30 min. (d) The octanal gel was removed with a scoop net. (e) Recovered octanal (24 mL, the recovery rate was of 80%) and powders by vacuum distillation. Photographs of (f) acid fuchsin and (g) cipro aqueous solution taken under 353 and 450 nm, respectively. The left side is before adsorption and the right side is after adsorption by D1 xerogel in these two sets of photographs. Fluorescence spectra of (h) acid fuchsin and (i) cipro solutions, respectively, incubated with D1 xerogel.

10. Dye adsorption capacities

10.1 Dye adsorption capacity of methylene blue

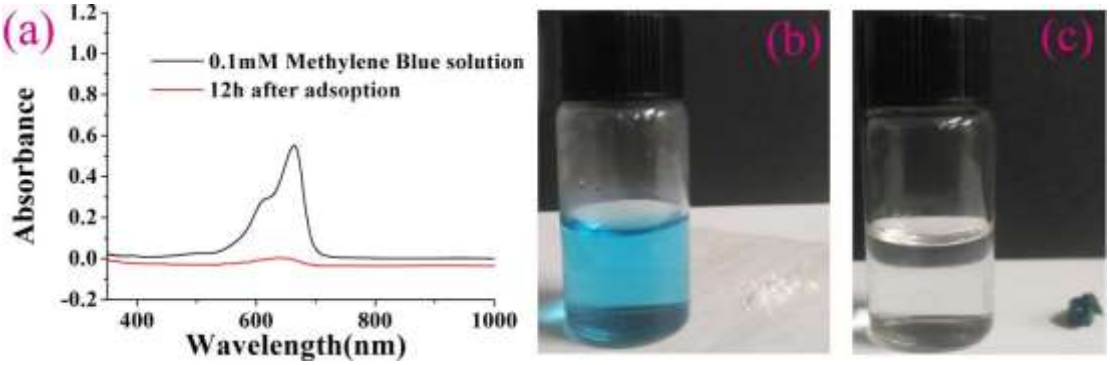

Figure S25. (a) UV/Vis spectrum of aqueous solution of methylene blue indicating the adsorption of methylene blue from water by acetonitrile xerogel of D1. Photograph of methylene blue solution before (b) and after (c) adsorption by acetonitrile xerogel of D1.

10.2 UV/Vis spectrum of different dye solution incubated with D1/acetonitrile xerogels

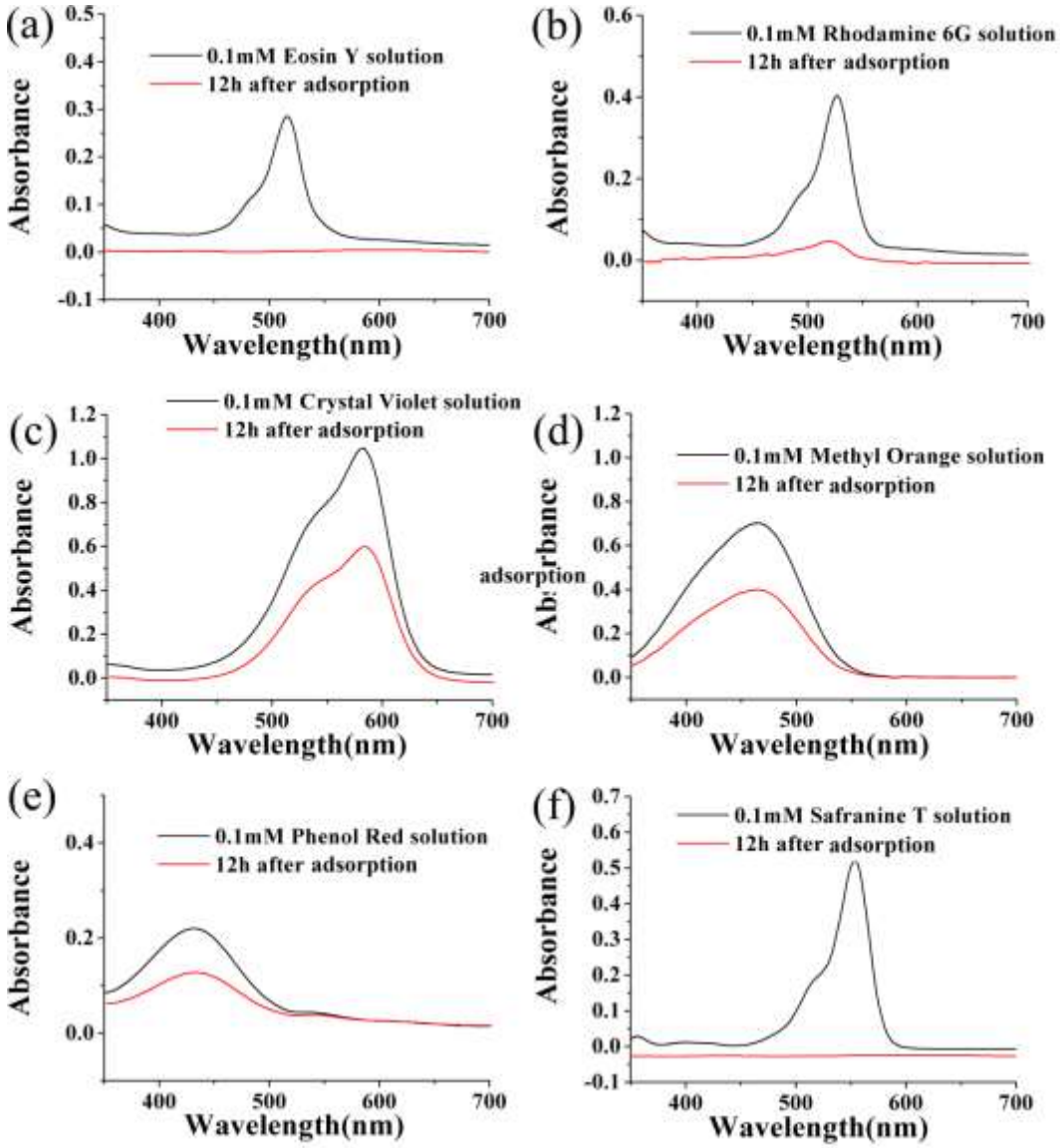

Figure S26. UV–vis spectra of the dye solutions incubated with D1/acetonitrile xerogels for (a) Eosin Y, (b) Rhodamine 6 G, (c) Crystal Violet, (d) Methyl Orange, (e) Phenol Red, (f) Safranine T.

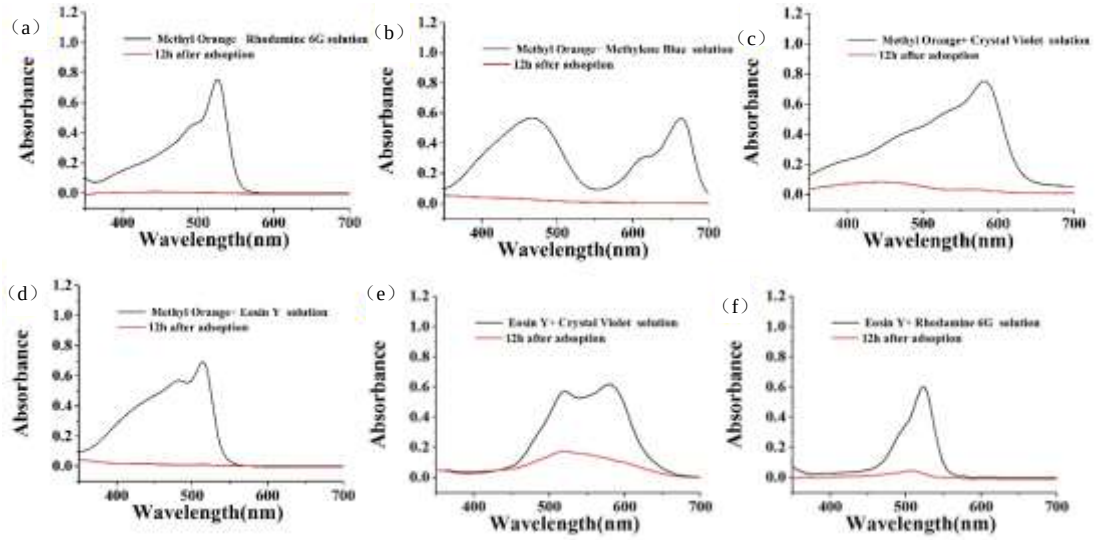

Figure S27. UV–vis spectra of the dye solutions incubated with D1/acetonitrile xerogels in a mixture of dyes. Method: the xerogels (10 mg) were immersed in 10 mL of a mixed dye solution prepared by mixing two dye solution with (0.05mM) in a 1:1 vol ratio.

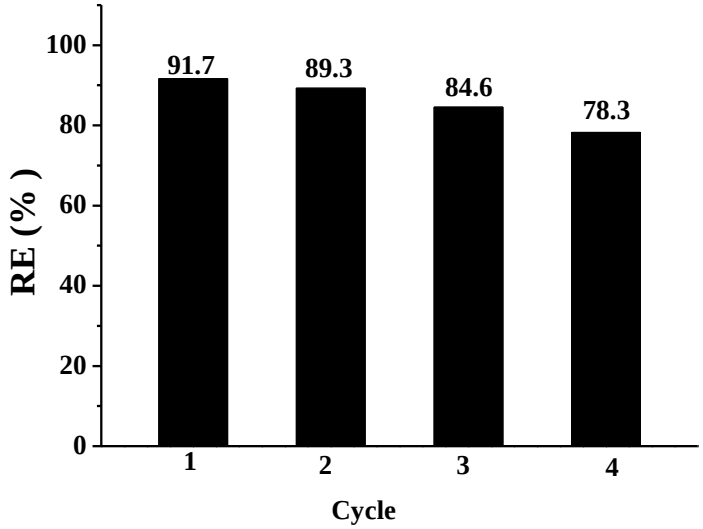

Figure S28. RE% obtained on recycling the D1/acetonitrile xerogels in the presence of MB at 25 °C.

The removal of dyes including methylene blue, eosin Y, rhodamine 6 G, crystal violet, methyl orange, phenol red and safranine T from water by the D1 xerogel was examined. Following the submergence of acetonitrile xerogel (20

mg) of D1 into an aqueous solution of dyes (5 ml, 0.2 mM), UV-visible spectroscopy revealed that some dye molecules (methylene blue, eosin Y, rhodamine 6 G and safranine T), were almost completely removed after 12h, whereas other dyes were partial removed.

The adsorption capacities of the gelator for methylene blue, crystal violet, phenol red, rhodamine 6 G, eosin Y, methyl orange and safranine T are 869.6m/g, 793.6mg/g, 750.4mg/g, 568mg/g, 852mg/g, 775mg/g and 638mg/g,respectively.

Method: The removal rate was calculated as $(c_0-c_e)/c_0$, where c_0 (mg L^{-1}) was the initial concentration of dye in the solution and c_e (mg L^{-1}) was the equilibrium concentration. The maximum amount of dyes adsorbed at equilibrium q^e (mg $g^{-1)}$ was calculated as:

$$q^e = (c_0-c_e)* V/W$$

where V (L) was the solution volume and W (g) was the mass of xerogel.

10.3 Photos of acid fuchsin solutions before and after absorption by D1 xerogel

Figure S29. Photos of the dye solutions before (a) and after (b) absorption by D1 xerogel, respectively.